Zhang and Peng
Protection and Control of Modern Power Systems (2023) 8:30
https://doi.org/10.1186/s41601-023-00303-z

Protection and Control of Modern Power Systems

ORIGINAL RESEARCH

Open Access

Adaptive H_∞ event-triggered load frequency control in islanded microgirds with limited spinning reserve constraints

Yajian Zhang[1] and Chen Peng[1*]

Abstract

Using an islanded microgrid (MG) with large-scale integration of renewable energy is the most popular way of solving the reliable power supply problem for remote areas and critical electrical users. However, compared with traditional power systems, the limited spinning reserves and network communication bandwidth may cause weak frequency stability in the presence of stochastic renewable active outputs and load demand fluctuations. In this paper, an adaptive event-triggered control (ETC) strategy for a load frequency control (LFC) system in an islanded MG is proposed. First, a bounded adaptive event-triggered communication scheme is designed. This not only saves on network resources, but also ensures that the control center has a sensitive monitoring ability for the MG operating status when the frequency deviations have been effectively damped. Secondly, by fully considering the spinning reserve constraints and uncertain communication delays, the LFC system is described as a nonlinear model with saturation terms. Design criteria for ETC parameters are strictly deduced based on Lyapunov stability theory. Finally, an ETC parameter optimization algorithm based on random direction search is developed to reconcile the bandwidth occupancy and control performance. The effectiveness of the proposed method is verified in an MG test system.

Keywords Microgrid, Load frequency control, Event-triggered control, Nonlinear saturation, Time delay

1 Introduction

Increased attention on carbon emissions has promoted the development of distributed generation technologies with sun and wind as the energy sources [1, 2]. Correspondingly, a microgrid (MG) which integrates large-scale distributed generators has become an important approach towards providing reliable power supply service for remote areas or sensitive loads [3–5]. However, because of the uncertainties in distributed generation and load demand fluctuations, the power supply and demand in an MG are often unmatched, which can cause an adverse effect on frequency stability [6–8]. Therefore, an MG control center is usually equipped with a load frequency control (LFC) system to regulate the active power outputs of generators according to the frequency deviation so that the power supply–demand balance can be maintained [9, 10].

It should be mentioned that compared to traditional power systems with large-capacity synchronous generators, the frequency stability in an MG is more vulnerable to the double challenges from physical and cyber layers. An MG is generally equipped with small-capability and low-inertia generators [11, 12], so that under the same level of power supply–demand imbalance, the frequency deviation in an MG is larger and the corresponding recovery time is longer than in a conventional power system [13, 14]. Hence, the use of energy storage systems (ESSs) to provide auxiliary frequency regulation services has attracted attention. For example, an MG frequency regulation scheme considering electric vehicle clusters

*Correspondence:
Chen Peng
c.peng@shu.edu.cn
[1] School of Mechatronic Engineering and Automation, Shanghai University, Shanghai, China

is proposed in [15], where the delay-independent control design criteria are strictly deduced based on Lyapunov stability theory. A delay-dependent sliding LFC strategy for an islanded MG containing ESSs and diesel generators is designed [16]. In the above works, the inverters in ESSs mainly adopt a constant-power control scheme with no inertia support for the MG. Therefore, some have proposed the virtual synchronous generator (VSG) control method for the inverters. By designing the algorithm to simulate the characteristics of synchronous generators, the inverters can provide extra inertia support for the MG [17]. A frequency regulation framework with VSG controlled ESSs is proposed to provide ancillary services in [18].

On the other hand, the MG control center must rely on the communication network to transmit control instructions and operating status with the equipment participating in the LFC. This will inevitably bring in uncertain time delay-induced problems [19]. Under the weakening inertia trend, the uncertain time delays will further enlarge the frequency deviations [20]. While the periodic triggered control (PTC) scheme is adopted in the above literature, the main drawback of PTC is that the operating status and control instructions are required to be transmitted over the network at each sampling period. This will cause a heavy communication burden in the MG. Therefore, some have proposed event triggered control (ETC) schemes, where the communication interaction is only triggered if the control performance has degenerated to under a preset threshold. The main objective of ETC is to reduce the communication frequency along with sacrificing partial dynamic performance [21–23]. With consideration of uncertain time delays, reference [24] deduces the ETC parameter criteria with a fixed triggered threshold by constructing a Lyapunov function. To further reduce the bandwidth occupancy, an adaptive event-triggered communication scheme is proposed where the triggered threshold is adaptively increased after frequency deviations have been well damped [25]. However, in existing adaptive ETC research, the exponential increase mechanism for adjusting the triggered threshold is usually adopted, while the upper bound of triggered threshold is restricted. That means that the triggered difficulty will rise rapidly when the frequency deviations start to be effectively damped. However, higher triggered difficulty will cause the MG control center to lose the monitoring sensitivity for operating status of the LFC system, resulting in slow recovery speed of frequency deviations. For a practical MG, continuous frequency deviation is deleterious to its safe and economic operation [26].

Most existing event-triggered LFC strategies have not taken the spinning reserve constraints of the MG into consideration. Spinning reserve is the maximum adjustable releasing or absorbing capability of the MG to maintain frequency stability. This is generally 10–20% of the total rated capacity of the MG. When the power supply–demand imbalance exceeds the spinning reserve limitation, the generation devices can only participate in LFC with their maximum adjustable capabilities. In other words, the power supply–demand imbalance can only be finitely reduced and the frequency deviations cannot be damped to zero. In this case, the MG control center should quickly adjust the control instruction to the maximum spinning reserve to dampen the frequency deviations as much as possible while avoiding the frequency deviation exceeding the allowable range. The current ETC schemes without considering the spinning reserve constraints may exhibit frequency over-limitation risk or a slow recovery problem [27].

Based on the above assessments, a bounded adaptive event-triggered LFC strategy considering spinning reserve constraints in islanded MGs is proposed in this paper, and the main contributions are as follows:

1. By fully taking the spinning reserve constraints into consideration, the networked LFC system with auxiliary VSG controlled ESSs is described as a nonlinear saturation model. Compared with current modelling methods without considering the spinning reserve constraints, the established model can exactly reflect the frequency dynamics of the actual MG.
2. A bounded adaptive ETC strategy is developed. Compared with the existing unbounded adaptive ETC methods, the triggered threshold in the proposed method is limited within a certain range to guarantee a sensitive monitoring ability of the MG operating status. By constructing a Lyapunov function considering time delays and spinning reserve limitations, the ETC parameter constraints with H_∞ damping performance to external power uncertainties are deduced. In addition, an ETC parameter optimization algorithm considering both cyber and control performances is developed.

The rest of the paper is organized as follows. Section 2 presents the LFC framework of islanded MG with limited spinning reserves. The design criteria and optimization algorithm are given in Section 3. Case studies are conducted in Section 4 to illustrate the effectiveness of the proposed method. Section 5 draws the conclusions.

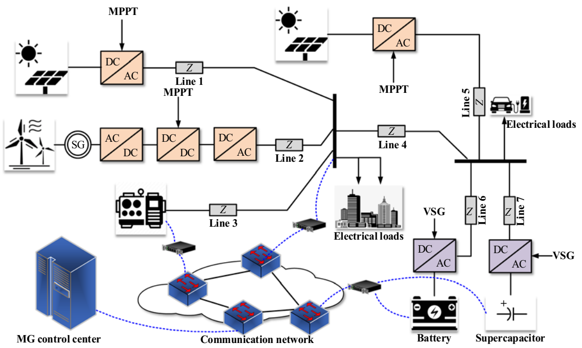

Fig. 1 Networked LFC system

2 LFC model in islanded MG with limited spinning reserves

2.1 LFC system with auxiliary VSG-controlled ESSs

As shown in Fig. 1, the power sources in an islanded MG contain wind turbines (WTs), photovoltaic plants (PVs), diesel generators (DGs) and ESSs. Considering weather unpredictability, the WTs and PVs generally do not participate in frequency regulation while injecting active power into the MG by adopting maximum power point tracking (MPPT) technology. The frequency regulation task is usually undertaken by the DGs and ESSs because of their controllable characteristics.

The detailed LFC mechanism in an islanded MG is as follows. The fluctuations of renewable generations or load demands will cause imbalance between the mechanical torque (produced by the prime motor and imposed on the rotating shaft of the synchronous generator) and the electromagnetic torque generated by the synchronous generator. Correspondingly, the rotational angular velocity of the synchronous generator (i.e., the frequency of the MG) will deviate from the rated value. In this case, the DG will adjust the mechanical power output by the primary motor to realize power supply–demand re-balance at the rated frequency point.

The above dynamic process can be described as a first-order inertial model. For a given power supply–demand imbalance, the frequency deviation and restoration speed are positively correlated to the damping and inertia of the synchronous generator in the DGs, respectively [19]. However, it should be noted that a high proportion of renewable generation integrated into the MG will reduce the installed capacities of the DGs equipped with synchronous generators. In this case, the frequency deviation, rate of change of frequency (RoCoF), and restoration speed will be enlarged. Therefore, in this paper, to provide auxiliary inertia and damping support for the MG, a VSG control strategy, which simulates the rotating characteristics of the synchronous generator, is adopted in the ESSs [28].

Assume that the amounts of DG and ESS in the islanded MG are N and M, respectively. Let H and D be the equivalent rotational inertia and damping coefficient of the MG. The relationships between (H, D) and each generation device are given by:

$$H = \sum_{n=1}^{N} H_{\mathrm{DG}n} \times \frac{S_{\mathrm{DG}n}}{S} + \sum_{n=1}^{M} H_{\mathrm{ESS}n} \times \frac{S_{\mathrm{ESS}n}}{S} \tag{1}$$

$$D = \sum_{n=1}^{N} D_{\mathrm{DG}n} \times \frac{S_{\mathrm{DG}n}}{S} + \sum_{n=1}^{M} D_{\mathrm{ESS}n} \times \frac{S_{\mathrm{ESS}n}}{S} \tag{2}$$

where $H_{\mathrm{DG}n}$ and $H_{\mathrm{ESS}m}$ are the inertia of the n^{th} DG and m^{th} VSG-controlled ESS, respectively, and $D_{\mathrm{DG}n}$ and $D_{\mathrm{ESS}m}$ are the corresponding damping coefficients. $S_{\mathrm{DG}n}$, $S_{\mathrm{ESS}m}$, and S are the rated capabilities of the n^{th} DG, m^{th} VSG-ESS and the total MG, respectively. The dynamics of the LFC system in an islanded MG with VSG-controlled ESSs can be described as [29–31]:

$$\begin{cases} \dot{x}(t) = Ax(t) + Bu(t) + Ew(t) \\ y(t) = Cx(t) \end{cases} \tag{3}$$

where $A = \begin{bmatrix} -\frac{D}{H} & A_{12} & 0 & A_{14} & 0 \\ 0 & A_{22} & A_{23} & 0 & 0 \\ A_{31} & 0 & A_{33} & 0 & 0 \\ 0 & 0 & 0 & A_{44} & 0 \\ 1 & 0 & 0 & 0 & 0 \end{bmatrix}$, $B = \begin{bmatrix} 0 \\ 0 \\ B_3 \\ B_4 \\ 0 \end{bmatrix}$,

$E = \begin{bmatrix} -\frac{1}{H} \\ 0 \\ 0 \\ 0 \\ 0 \end{bmatrix}$, $A_{12} = \left[\frac{1}{H}\right]_{1\times N}$, $A_{14} = \left[\frac{1}{H}\right]_{1\times M}$,

$A_{22} = -A_{23} = \mathrm{diag}\{-\frac{1}{T_{\mathrm{t}n}}\}$, $A_{31} = \left[-\frac{1}{T_{\mathrm{g}n} R_{\mathrm{DG}n}}\right]_{N\times 1}$,

$A_{33} = \mathrm{diag}\{-\frac{1}{T_{\mathrm{g}n}}\}$, $A_{44} = \mathrm{diag}\{-\frac{1}{T_{\mathrm{ESS}m}}\}$, $B_3 = \left[\frac{\alpha_n}{T_{\mathrm{g}n}}\right]_{N\times 1}$,

$B_4 = \left[\frac{\beta_m}{T_{\mathrm{ESS}m}}\right]_{M\times 1}$, $C = [1, 0, 0, 0, 0]$, and $x(t) = [\Delta f, \Delta P_{\mathrm{DG}1}, \ldots, \Delta P_{\mathrm{DG}N}, \Delta P_{\mathrm{v}1}, \ldots, \Delta P_{\mathrm{v}N}, \Delta P\mathrm{ref\ ESS}1, \ldots, \Delta P\mathrm{ref\ ESS}M, \Delta P_{\mathrm{ESS}1}, \ldots, \Delta P_{\mathrm{ESS}M}, \int \Delta f]^{\mathrm{T}}$. Δf is the frequency deviation, $\Delta P_{\mathrm{DG}n}$ ($n = 1, 2, \ldots, N$) and $\Delta P_{\mathrm{ESS}m}$ ($m = 1, 2, \ldots, M$) are the active power output increments of the n^{th} DG and m^{th} ESS, respectively. ΔPvn is the valve opening variation of the governor in the n^{th} DG, and $\Delta P\mathrm{ref\ ESS}m$ is the active power output instruction of the m^{th} ESS. u is the instruction of the spinning reserve injected into the MG, $w(t) = \Delta P_{\mathrm{WT}} + \Delta P_{\mathrm{PV}} - \Delta P_{\mathrm{D}}$ represent the external power uncertainties, ΔP_{WT} and ΔP_{PV} are the outputs of WTs and PVs, respectively, and ΔP_{D} are the load demands.

R_{DGn} is the droop coefficient of the DG, T_{ESSn} is the time constant of the inverter in the m^{th} ESS, whereas T_{gn} and T_{tn} are the time constants of the governor and diesel engine, respectively. α_n and β_m are the participation factors of the DG and ESS satisfying $\Sigma\alpha_n+\Sigma\beta_m=1$.

2.2 Bounded adaptive ETC scheme

To maintain power supply and demand balance at the rated frequency point, the MG control center usually adjusts the control instructions (i.e., the spinning reserve injected into the MG) according to the current operating status of the LFC systems. Clearly, the transmission of control instructions and operating status must rely on the communication network, so the inevitable transmission delays may adversely affect the stability of the LFC system or even cause an instability accident. To reduce the dependence on the network and guarantee a sensitive monitoring ability to the LFC system simultaneously, the following bounded adaptive event-triggered communication scheme is proposed:

$$\begin{aligned} t_{h+1}T_s = t_hT_s + \min\{l|e^T(i_lT_s)\Phi e(i_lT_s) \\ \geq \delta(t_hT_s)x^T(t_hT_s)\Phi x(t_hT_s)\} \end{aligned} \tag{4}$$

where t_hT_s is the triggered moment, $i_lTs=t_hT_s+lT_s$, $e(i_lT_s)=x(i_lT_s)\text{-}x(t_hT_s)$, Φ is the performance weighting matrix, and T_s is sampling period. $\delta(t_hT_s)=\min\{\delta_M, \max\{\delta_m, \nu\delta(t_{h-1}T_s)\}$ is the adaptive triggered threshold. The coefficient ν is given by:

$$\nu = \begin{cases} 0, ||y(t_{h+1}T_s)|| \geq ||y(t_hT_s)|| \\ 1-\frac{2\mu}{\pi}\text{atan}\left(\frac{||y(t_{h+1}T_s)||-||y(t_hT_s)||}{||y(t_hT_s)||}\right), \text{others} \end{cases} \tag{5}$$

where $\mu>0$ and δ_m, $\delta_M \in (0, 1)$, $\delta_m \leq \delta_M$. According to (5), the triggered threshold is limited within $[\delta_m, \delta_M]$.

Remark 1 Equation (4) shows that only when the weighting value of the difference between the sampled system status and the last triggered one is larger than the pre-set value then, and only then, can the current system status be transmitted to the control center through the network. If $\delta_m=\delta_M$, the bounded adaptive event-triggered communication scheme (4) is equivalent to a fixed-triggered threshold scheme. In particular, if $\delta_m=\delta_M=0$, the proposed bounded adaptive ETC scheme is equivalent to a periodical triggered one. In addition, when the system status of the LFC starts to be damped, the increasing rate of triggered threshold is characterized by the coefficient ν.

The state feedback control scheme is adopted in this paper. Since only the sampled system status satisfying the triggered condition (4) can be transmitted to the control center through the network, the control instruction update intervals are prolonged compared to the traditional periodic triggered control methods. In other words, the control instructions remain unchanged during two neighboring triggered moments. Hence, the ideal control instruction of spinning reserve injected into the MG satisfying $u(t)=Kx(t_hT_s)$, $t\in[t_hT_s+\tau_{t_h}, t_{h+1}T_s+\tau_{t_{h+1}}]$, where K and $\tau_{t_h} \in [0, \overline{\tau}]$ are the controller gain and transmission delay, respectively. Then the interval of two neighboring triggered moments can be divided into a series of subsets as $\Omega_h = \cup_{l=0}^{t_{h+1}-t_h-1}\Omega_h^l$, where $\Omega_h^l = [i_hT_s + \tau_{i_h}, (i_h+1)T_s + \tau_{i_h+1})$ and $i_h = t_kh + lh$. Defining $\tau(t)=t\text{-}i_hT_s$ satisfying $0 \leq \tau(t) \leq \overline{\tau} + T_s \triangleq d$, the ideal control instruction of spinning reserve injected into the MG is equivalent to $u(t)=K[x(t\text{-}\tau(t))\text{-}e(i_hT_s)]$, $t\in\Omega_h^l$.

However, because of the generation rate constraints of DGs and capacity limitations of inverters, the adjustable spinning reserves of the MG are always limited. If the power supply–demand imbalance exceeds the maximum spinning reserve constraints, the imbalance can only be finitely reduced. In this case, each generation device participated in the LFC can only provide the maximum regulation capacity (i.e., inject external power into or absorb redundant power from the MG). Therefore, the actual spinning reserve provided for the LFC system can be described as the following nonlinear saturation model:

$$\begin{aligned} u(t) &= \begin{cases} \Delta P_{r\max}, Kx(t-\tau) \geq \Delta P_{r\max} \\ Kx(i_hT_s), -\Delta P_{r\max} \leq Kx(t-\tau) \leq \Delta P_{r\max} \\ -\Delta P_{r\max}, Kx(t-\tau) \leq -\Delta P_{r\max} \end{cases} \\ &= K[x(t-\tau(t)) - e(i_hT_s)] + \varphi(Kx(i_hT_s)) \end{aligned} \tag{6}$$

where $\Delta P_{r\max}$ is the maximum allowable spinning reserve in the MG, and $\phi(\cdot)$ is the function describing nonlinear saturation characteristics of spinning reserve constraints. Finally, the close-loop dynamics of the LFC system in an islanded MG adopting the proposed unbounded adaptive event-triggered communication scheme (4) can be described as:

$$\dot{x}(t) = Ax(t) + BK[x(t-\tau(t)) - e(i_hT_s)] + Ew(t) + B\varphi(Kx(i_hT_s)) \tag{7}$$

Remark 2 The nonlinear saturation item $\phi(Kx(i_hT_s))$ can be explained from Fig. 2. The abscissas of the intersection points of $\phi(Kx(i_hT_s))$ and $Kx(i_hT_s)$ are the maximum allowable spinning reserves of the MG. The dashed line represents the function $g(Kx(i_hT_s))=\text{-}\lambda Kx(i_hT_s)$ with

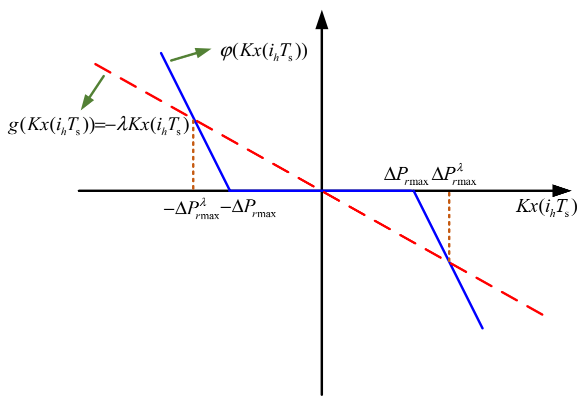

Fig. 2 Saturation model of spinning reserve constraints

$\lambda \in [0, 1]$. Let $-\Delta P\lambda$ $r$max, $\Delta P\lambda$ $r$max be the abscissas of the intersection points of $g(Kx(i_hT_s))$ and $\phi(Kx(i_hT_s))$, satisfying $\Delta P\lambda$ $r\max = \Delta P_{r\max}/(1-\lambda)$. From Fig. 2, it can be seen that $[-\Delta P_{r\max}, \Delta P_{r\max}] \subseteq [-\Delta P\lambda$ $r$max, $\Delta P\lambda$ $r$max$]$. Clearly, there are:

$$\begin{cases} -\lambda Kx(i_hT_s) \le \varphi(Kx(i_hT_s)) \le 0,\ 0 \le Kx(i_hT_s) \le \Delta P_{r\max} \\ 0 \le \varphi(Kx(i_hT_s)) \le -\lambda Kx(i_hT_s),\ -\Delta P_{r\max} \le Kx(i_hT_s) \le 0 \end{cases} \tag{8}$$

Hence, for an arbitrary positive defined matrix Ξ, the following inequality always holds:

$$\varphi^{\mathrm{T}}(Kx(i_hT_s))\Xi(\varphi(Kx(i_hT_s)) + \lambda Kx(i_hT_s)) \le 0 \tag{9}$$

3 Optimal design for ETC parameters

For the LFC system in the MG, the ETC parameters should satisfy the following three requirements:

1. The closed-loop LFC system described in (7) should be asymptotically stable if the external power uncertainties $w(t) = 0$.
2. The LFC system should have an H_∞ damping performance to the external power uncertainties, i.e., the output of the LFC system should satisfy $||y(t)||_2 \le \gamma ||w(t)||_2$, where $w(t) \in L_2[0, \infty)$ and $\gamma > 0$ is the damping coefficient.
3. To guarantee safe operation of the MG system, the frequency deviation under uncertain time delays and external power fluctuations must be limited within the allowable ranges.

In this section, the constraints of ETC parameters are first deduced by adopting Lyapunov stability theory. Then an optimization algorithm for the ETC parameters is developed to improve the dynamic performance under uncertain communication delays and external power fluctuations.

3.1 Design criteria of ETC parameters

Theorem 1 (Closed-loop stability criteria under spinning reserve constraints) *For given scalars ρ, γ, δ_M, λ, $d > 0$, if there exist matrices X, Ξ and positive definite matrices P, Q, R, Φ satisfying* (10) *and* (11), *then the closed-loop LFC system* (7) *with the proposed bounded adaptive event-triggered communication scheme* (4) *is H_∞ asymptotically stable under uncertain communication delays and external power fluctuations.*

$$\begin{bmatrix} R & X \\ X^{\mathrm{T}} & R \end{bmatrix} \ge 0 \tag{10}$$

$$\begin{bmatrix} \Omega_{11} & \Omega_{12} & \Omega_{13} & \Omega_{14} & \Omega_{15} & \Omega_{16} & \Omega_{17} & \Omega_{18} \\ * & \Omega_{22} & \Omega_{23} & 0 & 0 & 0 & 0 & 0 \\ * & * & \Omega_{33} & \Omega_{34} & 0 & \Omega_{36} & \Omega_{37} & 0 \\ * & * & * & \Omega_{44} & 0 & \Omega_{46} & \Omega_{47} & 0 \\ * & * & * & * & \Omega_{55} & 0 & \Omega_{57} & 0 \\ * & * & * & * & * & \Omega_{66} & \Omega_{67} & 0 \\ * & * & * & * & * & * & \Omega_{77} & 0 \\ * & * & * & * & * & * & * & \Omega_{88} \end{bmatrix} \le 0 \tag{11}$$

where $\Omega_{11} = Q - R + PA + A^TP$, $\Omega_{12} = X^T$, $\Omega_{13} = PBK - X^T + R$, $\Omega_{14} = -PBK$, $\Omega_{15} = PE$, $\Omega_{16} = PB$, $\Omega_{17} = A^TP$, $\Omega_{18} = C^T$, $\Omega_{22} = -Q - R$, $\Omega_{23} = R - X$, $\Omega_{33} = -2R + X^T + X + \delta_M\Phi$, $\Omega_{34} = -\delta_M\Phi$, $\Omega_{36} = -\lambda K^T\Xi$, $\Omega_{37} = K^TB^TP$, $\Omega_{44} = -\Phi + \delta_M\Phi$, $\Omega_{46} = \lambda K^T\Xi$, $\Omega_{47} = -K^TB^TP$, $\Omega_{55} = -\gamma^2 I$, $\Omega_{57} = E^TP$, $\Omega_{66} = -2\Xi$, $\Omega_{67} = B^TP$, $\Omega_{77} = \rho^2d^2R\text{-}2\rho P$, $\Omega_{88} = -I$.

Proof Choose the following Lyapunov function:

$$\begin{aligned} V(t) &= x^{\mathrm{T}}(t)Px(t) + \int_{t-d}^{t} x^{\mathrm{T}}(s)Qx(s)\mathrm{d}s \\ &\quad + d\int_{-d}^{0}\int_{t+r}^{t} \dot{x}^{\mathrm{T}}(s)R\dot{x}(s)\mathrm{d}s\mathrm{d}r \end{aligned} \tag{12}$$

According to event-triggered communication scheme (4), $e^{\mathrm{T}}(i_lT_s)\Phi e(i_lT_s) \le \delta_M x^{\mathrm{T}}(t_hT_s)\Phi x(t_hT_s)$ holds during two neighboring triggered moments. Applying (9), Jensen's inequality [32] and reciprocally convex theorem [33], if there exists a matrix X with suitable dimensions, the time derivative of $V(t)$ satisfies:

$$\begin{aligned}\dot{V}(t) &\leq \dot{x}^{\mathrm{T}}(t)Px(t) + x^{\mathrm{T}}(t)P\dot{x}(t) + x^{\mathrm{T}}(t)Qx(t) - x^{\mathrm{T}}(t-d)Qx(t-d) \\ &+ d^2\dot{x}^{\mathrm{T}}(t)R\dot{x}(t) - \begin{bmatrix} x(t-\tau(t)) - x(t-d) \\ x(t) - x(t-\tau(t)) \end{bmatrix}^{\mathrm{T}} \begin{bmatrix} R & X \\ X^{\mathrm{T}} & R \end{bmatrix} \begin{bmatrix} x(t-\tau(t)) - x(t-d) \\ x(t) - x(t-\tau(t)) \end{bmatrix} \\ &+ y^{\mathrm{T}}(t)y(t) - \gamma^2 w^{\mathrm{T}}(t)w(t) + \delta_M x^{\mathrm{T}}(t-\tau(t))\Phi x(t-\tau(t)) \\ &- e^{\mathrm{T}}(i_l T_{\mathrm{s}})\Phi e(i_l T_{\mathrm{s}}) - 2\varphi^T(Kx(i_h T_{\mathrm{s}}))\Xi(\varphi(Kx(i_h T_{\mathrm{s}})) + \lambda Kx(i_h T_{\mathrm{s}})) \\ &- y^{\mathrm{T}}(t)y(t) + \gamma^2 w^{\mathrm{T}}(t)w(t)\end{aligned} \tag{13}$$

Defining $\xi(t)=[x^{\mathrm{T}}(t), x^{\mathrm{T}}(t\text{-}d), x^{\mathrm{T}}(t\text{-}\tau(t)), e^{\mathrm{T}}(i_h T_s), w^{\mathrm{T}}(t), \phi^{\mathrm{T}}(Kx(i_h T_s))]^{\mathrm{T}}$, there are:

$$\begin{aligned} x(t) &= [I\ \ 0\ \ 0\ \ 0\ \ 0\ \ 0]\xi(t) = e_1\xi(t) \\ \dot{x}(t) &= [A\ \ 0\ \ BK\ \ -BK\ \ H\ \ B]\xi(t) = e_2\xi(t) \\ x(t-d) &= [0\ \ I\ \ 0\ \ 0\ \ 0\ \ 0]\xi(t) = e_3\xi(t) \\ x(t-\tau(t)) &= [0\ \ 0\ \ I\ \ 0\ \ 0\ \ 0]\xi(t) = e_4\xi(t) \\ e(i_l T_s) &= [0\ \ 0\ \ 0\ \ I\ \ 0\ \ 0]\xi(t) = e_5\xi(t) \\ w(t) &= [0\ \ 0\ \ 0\ \ 0 I\ \ 0]\xi(t) = e_6\xi(t) \\ \varphi(Kx(i_h T_s)) &= [0\ \ 0\ \ 0\ \ 0\ \ 0\ \ I]\xi(t) = e_7\xi(t) \\ y(t) &= [C\ \ 0\ \ 0\ \ 0\ \ 0\ \ 0]\xi(t) = e_8\xi(t) \end{aligned}$$

If the inequality (14) holds, there is $\dot{V}(t) \leq -y^{\mathrm{T}}(t)y(t) + \gamma^2 w^{\mathrm{T}}(t)w(t)$.

$$\begin{aligned} & e_2^{\mathrm{T}}Pe_1 + e_1^{\mathrm{T}}Pe_2 + e_1^{\mathrm{T}}Qe_1 - e_3^{\mathrm{T}}Qe_3 + d^2 e_2^{\mathrm{T}}Re_2 \\ & - \begin{bmatrix} e_4 - e_3 \\ e_1 - e_4 \end{bmatrix}^{\mathrm{T}} \begin{bmatrix} R & X \\ X^{\mathrm{T}} & R \end{bmatrix} \begin{bmatrix} e_4 - e_3 \\ e_1 - e_4 \end{bmatrix} + e_8^{\mathrm{T}}e_8 - \gamma^2 e_6^{\mathrm{T}}e_6 \\ & + \delta_M e_4^{\mathrm{T}}\Phi e_4 - e_5^{\mathrm{T}}\Phi e_5 - 2e_7^{\mathrm{T}}\Xi(e_7 + \lambda K(e_4 - e_5)) \\ & \leq 0 \end{aligned} \tag{14}$$

Clearly, $\dot{V}(t) \leq 0$ always holds when $w(t)=0$. In addition, under the zero initial condition, $\int_0^{+\infty} y^{\mathrm{T}}(t)y(t)\mathrm{d}t \leq \gamma^2 \int_0^{+\infty} w^{\mathrm{T}}(t)w(t)\mathrm{d}t$ holds, i.e., $||y(t)||_2 \leq \gamma||w(t)||_2$. This means that the closed-loop LFC system with spinning reserve constraints is H_∞ asymptotically stable. Moreover, inequalities (11) and (14) are equivalent. Thus this completes the proof.

Because of the existence of nonlinear items (e.g., Ω_{13}, Ω_{14}, Ω_{36}), inequality (10) is in a bilinear matrix inequality (BLMI) form which is difficult to solve. Therefore, the congruent transformation approach is adopted in this paper. Define $\Lambda=P^{-1}$, $\Psi=\Omega^{-1}$, $K\Lambda=\Gamma$, $\tilde{Q} = \Lambda Q\Lambda$, $\tilde{R} = \Lambda R\Lambda$, $\tilde{\Phi} = \Lambda\Phi\Lambda$, $\tilde{X} = \Lambda X\Lambda$. By pre- and post-multiplying both sides of (10) and (11) with diag{Λ, Λ} and diag{Λ, Λ, Λ, Λ, I, Ξ^{-1}, Λ, I} respectively, the following corollary is obtained.

Corollary 1 *For given scalars ρ, γ, δ_M, λ, $d>0$, if there exist matrices X and positive definite matrices Λ, Ψ, $\tilde{Q}$, $\tilde{R}$ and $\tilde{\Phi}$ satisfying* (15) *and* (16), *then the closed-loop LFC system* (7) *with the proposed bounded event-triggered communication scheme* (4) *is H_∞-asymptotical. The controller gain is given by $K=\Gamma\Lambda^{-1}$ and the performance weighting matrix is given by $\Phi = \Lambda^{-1}\tilde{\Phi}\Lambda^{-1}$.*

$$\begin{bmatrix} \tilde{R} & \tilde{X} \\ \tilde{X}^{\mathrm{T}} & \tilde{R} \end{bmatrix} \geq 0 \tag{15}$$

$$\begin{bmatrix} \tilde{\Omega}_{11} & \tilde{\Omega}_{12} & \tilde{\Omega}_{13} & \tilde{\Omega}_{14} & \tilde{\Omega}_{15} & \tilde{\Omega}_{16} & \tilde{\Omega}_{17} & \tilde{\Omega}_{18} \\ * & \tilde{\Omega}_{22} & \tilde{\Omega}_{23} & 0 & 0 & 0 & 0 & 0 \\ * & * & \tilde{\Omega}_{33} & 0 & 0 & \tilde{\Omega}_{36} & \tilde{\Omega}_{37} & 0 \\ * & * & * & \tilde{\Omega}_{44} & 0 & \tilde{\Omega}_{46} & \tilde{\Omega}_{47} & 0 \\ * & * & * & * & \tilde{\Omega}_{55} & 0 & \tilde{\Omega}_{57} & 0 \\ * & * & * & * & * & \tilde{\Omega}_{66} & \tilde{\Omega}_{67} & 0 \\ * & * & * & * & * & * & \tilde{\Omega}_{77} & 0 \\ * & * & * & * & * & * & * & \tilde{\Omega}_{88} \end{bmatrix} \leq 0 \tag{16}$$

where $\tilde{\Omega}_{11} = \tilde{Q} - \tilde{R} + AP + PA^{\mathrm{T}}$, $\tilde{\Omega}_{12} = \tilde{X}^{\mathrm{T}}$, $\tilde{\Omega}_{14} = -\tilde{X}^{\mathrm{T}} + \tilde{R} + B\Gamma$, $\tilde{\Omega}_{15} = -B\Gamma$, $\tilde{\Omega}_{16} = E$, $\tilde{\Omega}_{17} = B\Psi$, $\tilde{\Omega}_{18} = \Lambda C^{\mathrm{T}}$, $\tilde{\Omega}_{22} = -\tilde{R} - \tilde{Q}$, $\tilde{\Omega}_{33} = -2\tilde{R} + \tilde{X}^{\mathrm{T}} + \tilde{X} + \delta_M\tilde{\Phi}$, $\tilde{\Omega}_{34} = -\delta_M\tilde{\Phi}$, $\tilde{\Omega}_{36} = -\lambda\Gamma^{\mathrm{T}}$, $\tilde{\Omega}_{37} = \Gamma^{\mathrm{T}}B^{\mathrm{T}}$, $\tilde{\Omega}_{44} = -\tilde{\Phi} + \delta_M\tilde{\Phi}$, $\tilde{\Omega}_{46} = \lambda\Gamma^{\mathrm{T}}$, $\tilde{\Omega}_{47} = -\Gamma^{\mathrm{T}}B^{\mathrm{T}}$, $\tilde{\Omega}_{55} = -\gamma^2 I$, $\tilde{\Omega}_{57} = -H^{\mathrm{T}}$, $\tilde{\Omega}_{66} = -2\Psi$, $\tilde{\Omega}_{67} = \Psi B^{\mathrm{T}}$, $\tilde{\Omega}_{77} = \rho^2 d^2\tilde{R} - 2\rho\Lambda$, $\tilde{\Omega}_{88} = -I$.

3.2 Optimization algorithm

The design criteria of controller gain K and performance weighting matrix Φ under given H_∞ damping coefficient and upper triggered threshold bound δ_M have been discussed in Sect. 2.1. However, the dynamic performance and triggered frequency are contradictory designing requirements in event-triggered LFC systems.

Specifically, more satisfied dynamic performance usually requires more frequent communications [34], which will increase the burden of the communication network in the MG. Therefore, an optimization algorithm is designed in this subsection to reconcile the conflict between bandwidth occupancy and dynamic control performance. The following objective function is chosen:

$$J(K,\delta_m,\delta_M,\Phi)|_{|\Delta f|\leq 0.1\%|\Delta f|_{\max}} = \sigma_1\frac{C_{\text{triggered}}}{C_\Sigma} + \sigma_2\frac{|\Delta f|_{\max}}{|\Delta f|_{\max\_\text{rated}}} \tag{17}$$

where σ_1 and σ_2 are the weighting coefficients satisfying $\sigma_1+\sigma_2=1$. $C_{\text{triggered}}$ is the triggered times during the frequency regulation process, and C_Σ is the total number of sampling periods. $|\Delta f|_{\max}$ is the maximum frequency deviation, and $|\Delta f|_{\max\_\text{rated}}$ is the allowable maximum frequency deviation.

From Corollary 1, the controller K and weighting matrix Φ can be directly obtained with given triggered threshold bounds (δ_m, δ_M). It means that the actual decision variables in objective function (17) are (δ_m, δ_M). For such a two-dimensional optimization problem, a random direction search algorithm is developed taking advantage of its fast convergence speed [35]. The proposed optimization algorithm includes the following steps:

Step 1 Input system matrices (A, B, C, E), allowable maximum spinning reserve $\Delta P_{r\max}$, upper delay bound d, maximum allowable frequency deviation $|\Delta f|_{\max\_\text{rated}}$, H_∞ performance index γ, weighting coefficients (σ_1, σ_2), initial triggered threshold boundaries [δ_{m0}, δ_{M0}], ($\delta_{m0}\leq\delta_{M0}$), step size $\theta>0$, scaling factor {$\varepsilon_{\min}$, $\varepsilon_{\max}$}, ($0<\varepsilon_{\min}<1$, $\varepsilon_{\max}>1$), termination threshold of iteration χ.

Step 2 Calculate the controller gain K_0 and performance weighting matrix Φ_0 under given δ_{M0} by using Corollary 1. Then calculate the corresponding value (denoted as J_0) of objective function (16).

Step 3 Randomly generate H unit vectors satisfying $\{(g_{mh},g_{Mh})|\sqrt{g_{mh}^2+g_{Mh}^2}=1,\ h=1,2,\ldots,H\}$. Then update the triggered threshold boundaries as follows:

$$\delta_{mh} = \delta_{m0} + \theta g_{mh} \tag{18}$$

$$\delta_{Mh} = \delta_{M0} + \theta g_{Mh} \tag{19}$$

Step 4 For each [$\delta_{mh'}$, $\delta_{Mh'}$] ($h'\in\{1, 2, \ldots, H'\}\subseteq\{1, 2, \ldots, H\}$) satisfying $0\leq\delta_{mh'}\leq\delta_{Mh'}\leq 1$, calculate the controller gain $K_{h'}$ and weighting performance matrix $\Phi_{h'}$ by applying Corollary 1. Then calculate the corresponding objective function value (denoted as $\{J_{h'}\}$), and obtain the optimal feasible solution [δ_{ml}, δ_{Ml}], $l\in\{1, 2, \ldots, H'\}$ with the minimal objective function value in current iteration.

Step 5 If $J_l<J_0$, then $\delta_{ml}\to\delta_{m0}$, $\delta_{Ml}\to\delta_{M0}$ and $\theta=\varepsilon_{\max}\theta$. Otherwise, keep δ_{m0} and δ_{M0} unchanged and let $\theta=\varepsilon_{\min}\theta$.

Step 6 If $|J_l$-$J_0|<\chi$, then output [δ_{m0}, δ_{M0}], K_0, and Φ_0. Otherwise, repeat **Steps 2–5**.

4 Case studies and discussions

In this section, the effectiveness of the proposed unbounded adaptive ETC method is verified in an islanded MG test system shown in Fig. 3. The simulated MG system contains one DG and one ESS, and the simulation parameters are listed in Table 1. The DG and VSG-controlled ESS are responsible for damping the frequency deviation caused by the uncertain electrical load demand and renewable generation fluctuations to zero via the proposed LFC scheme.

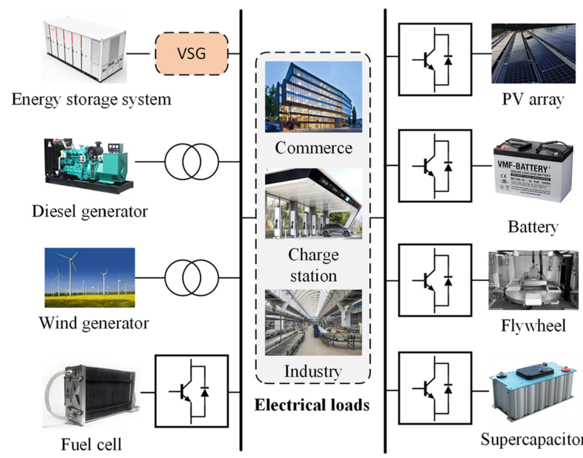

Fig. 3 Topology of the MG test system

Table 1 Simulation parameters

Parameters	Values
Equivalent rotational inertia ($2H$)	3 p.u.·s
Equivalent damping coefficient (D)	1 p.u.·Hz
Droop coefficient of DG (R_{DG})	3 Hz/p.u
Time constant of governor (T_g)	0.08 s
Time constant of turbine (T_t)	0.4 s
Time constant of ESS (T_{ESS})	0.04 s
Maximum spinning reserve ($\Delta P_{r\max}$)	0.2 p.u
Participation factors (α, β)	(0.7, 0.3)
Rated capacities (S_{DG}, S_{ESS})	200, 45 kVA
Maximum delay (d)	50 ms
Maximum rated frequency deviation ($|\Delta f|_{\max\_\text{rated}}$)	0.2 Hz
H_∞ damping coefficient (γ)	7.5
Weighting coefficients (σ_1, σ_2)	(0.3, 0.7)
Step size (θ)	0.001
Termination threshold of iteration (χ)	0.001
Scaling factor ($\varepsilon_{\min}$, $\varepsilon_{\max}$)	(0.7, 1.3)
Sampling period (T_s)	0.1 s

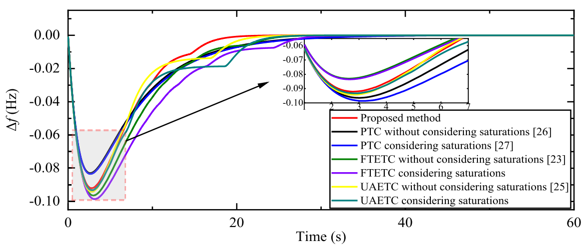

Fig. 4 Frequency deviations with different control schemes (step power fluctuation scenario)

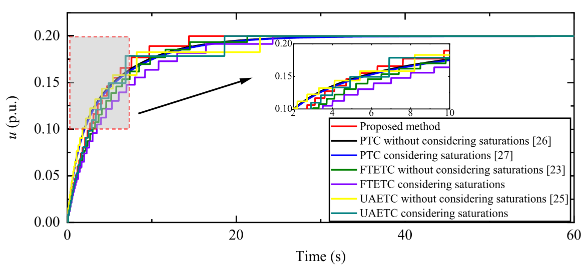

Fig. 5 Instructions of spinning reserves injected into MG with different control schemes (step power fluctuation scenario)

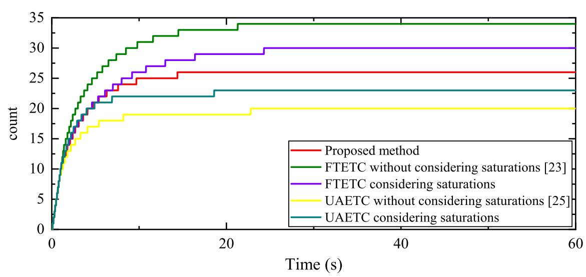

Fig. 6 Cumulative triggered times with different ETC schemes (step power fluctuation scenario)

4.1 Control performance with different control schemes

The ETC parameters are optimized under the external step power disturbance of $w(t) = -0.2$ p.u., as: $[\delta_m, \delta_M] = [0.005, \ 0.01]$, $K = [-1.1459, \ -0.2503, \ -0.3366, -0.7073, -0.4465]$, and

$$\Phi = \begin{bmatrix} 76.7023 & 18.9487 & 20.4452 & 30.4929 & 19.5897 \\ 18.9487 & 9.3862 & 3.5811 & 8.5611 & 5.5355 \\ 20.4452 & 3.5811 & 10.7711 & 8.8567 & 5.5355 \\ 30.4929 & 8.5611 & 8.8567 & 19.4274 & 8.7429 \\ 19.5897 & 5.5355 & 5.5355 & 8.7429 & 7.1263 \end{bmatrix}.$$

The following schemes are chosen for comparison. It should be mentioned that all the compared schemes have not taken the comprehensive performance improvement into consideration.

1. Periodic triggered control (PTC) without considering saturation [26];
2. Periodic triggered control (PTC) considering saturation [27];
3. Fixed-threshold ETC (FTETC) without considering saturation [23];
4. Fixed-threshold ETC (FTETC) considering saturation designed based on Corollary 1;
5. Unbounded adaptive ETC (UAETC) without considering saturation [25];
6. Unbounded adaptive ETC (UAETC) considering saturation designed based on Corollary 1.

4.1.1 *Step power fluctuation scenario*

Without losing generality, we assume that the external power disturbance $w(t)$ occurs with a -0.2 p.u. step change at $t = 0$ s. The frequency deviations with different control schemes are shown in Fig. 4. The instructions of spinning reserves injected into the MG are shown in Fig. 5, while Fig. 6 illustrates the cumulative triggered times with different ETC schemes. To assess the control performance of the LFC system, the frequency deviation ($|\Delta f|_{max}$), peak time (t_{peak}), settling time ($t_{settling}$), final triggered time and the integral absolute error (IAE) of frequency deviation are selected. Table 2 demonstrates the performance indices with different control schemes.

Table 2 Performance indices of different control schemes (step power fluctuation scenario)

Control schemes	$\lvert\Delta f\rvert_{max}$ (Hz)	t_{peak} (s)	$t_{settling}$ (s)	Triggered times	IAE (Hz s)
Proposed method	0.09209	2.76	18.36	26	0.07184
PTC without considering saturations [27]	0.08300	2.61	28.66	600	0.07834
PTC considering saturations [26]	0.08353	2.64	29.84	600	0.08073
FTETC without considering saturations [23]	0.09646	2.98	23.92	34	0.08739
FTETC considering saturations	0.09864	3.11	27.48	30	0.10233
UAETC without considering saturations [25]	0.09427	2.82	21.27	20	0.07504
UAETC considering saturations	0.09331	2.87	23.58	23	0.08528

For the same ETC schemes, it can be seen from Figs. 4, 5, 6 and Table 2 that there exist significant differences of the cumulative triggered times and control performance between considering and without considering the spinning reserve constraints. Compared with the case adopting the FTETC scheme considering the spinning reserve constraints, the control center adopting the FTETC scheme without considering the constraints will be triggered an extra four times during the time interval of [0, 60 s]. The corresponding frequency deviation of the FTETC scheme without considering the spinning reserve constraints can be reduced by 2.21% compared with the case considering the constraints. However, opposite conclusions can be obtained for the UAETC schemes considering or without considering the spinning reserve constraints compared with FTETC schemes. The above results show that whether the saturation limitations are taken into consideration has no obvious positive or negative contribution on the cumulative trigger time and control performance when designing the ETC system. This is because the current ETC design methods only focus on the feasibility analysis of ETC parameters while usually ignoring the comprehensive performance improvement of bandwidth occupancy and dynamic control performance.

Moreover, since an optimization algorithm is developed to reconcile the bandwidth occupancy and dynamic control performance, the proposed bounded adaptive ETC scheme has the minimal peak time, settling time and IAE in all the control methods. In addition, according to Fig. 5, the proposed method can approach the active power vacancy faster. Compared with the two periodic triggered control schemes, the frequency deviations with the proposed method have risen by no more than 10.95% while the triggered times are decreased by 95.67%. Compared with the fixed-threshold ETC schemes, the triggered times with the proposed bounded adaptive ETC scheme are reduced by over 13.33% since the threshold value is properly improved after the frequency deviation is effectively damped. In addition, although the triggered times of the proposed method are 30% larger than the unbounded adaptive ETC schemes, the settling times are shortened by 13.68% at least. The reason is that in the unbounded adaptive ETC schemes, the triggered difficulty rises rapidly because of the continuously increased threshold value. In this case, the control center cannot obtain the operating status of the LFC system in time. Therefore, the simulation results show that the proposed method not only saves network resources effectively, but also guarantees a satisfactory recoverability for the frequency deviations.

4.1.2 Random over-saturating power fluctuation scenario

In Sect. 4.1.1, the effectiveness of the proposed method was tested in the case that the external power uncertainties do not exceed the allowable maximum spinning reserve. In this subsection, frequency control performance of each scheme is further simulated and analyzed in a random power fluctuation scenario where the fluctuation amplitude may exceed the spinning reserve constraints. The load demands and active renewable generations are presented in Fig. 7. One can see from Fig. 7 that the changes of the external power fluctuations at $t=20$ s and 60 s are about 0.3 p.u. and -0.65 p.u., respectively, which are larger than the maximum available spinning reserve.

The frequency deviations and spinning reserves injected to the MG with different control schemes are demonstrated in Figs. 8 and 9, respectively. Figure 10 illustrates the triggered times and intervals with different ETC schemes. Variance ($S^2_{\Delta f}$), final triggered times and the IAE of frequency deviations are selected to assess the control performance, as demonstrated in Table 3 for the different control schemes.

According to Figs. 7 and 8, since the external power uncertainties exceed the maximum spinning reserve, the MG system can only provide the maximum regulation

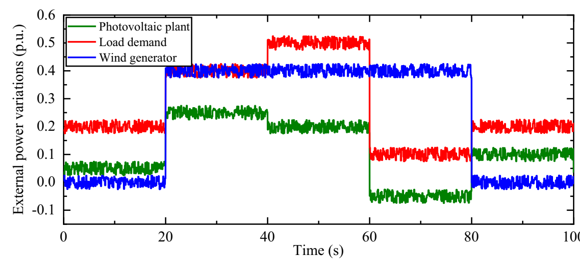

Fig. 7 Stochastic power variations

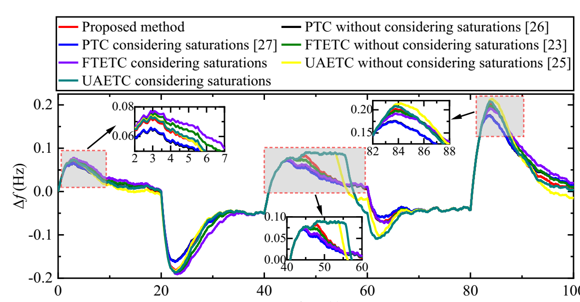

Fig. 8 Frequency deviations with different control schemes (random power fluctuation scenario)

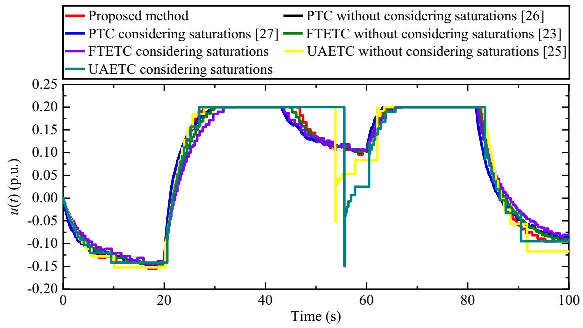

Fig. 9 Instructions of spinning reserves injected into the MG with different control schemes (random power fluctuation scenario)

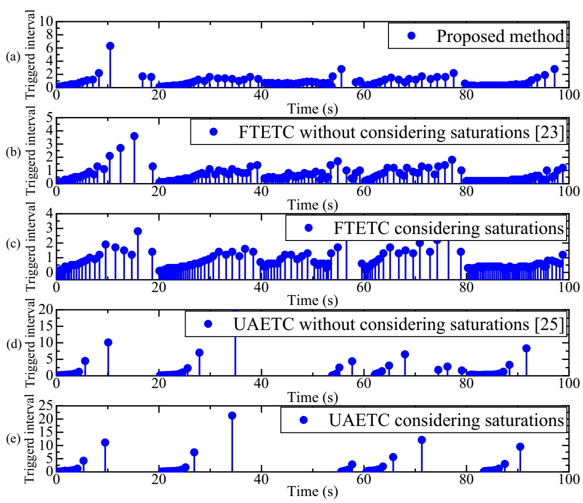

Fig. 10 Triggered intervals with different ETC schemes (random power fluctuation scenario)

capability for the LFC system during the time intervals as [20 s, 40 s] and [60 s, 80 s]. Correspondingly, the frequency deviations cannot be controlled to zero during the above two intervals. Compared with the periodical triggered control schemes, although the frequency deviation variance with the proposed method rises by 17.7%, the communication triggered times are reduced by 84.4%. In addition, compared with other ETC schemes, since the proposed method takes both control performance and bandwidth utilization into consideration, the frequency deviation variance and the IAE index are reduced by 13.11% and 6.077%, respectively.

Although Table 3 shows that the trigger times with unbounded adaptive ETC schemes are reduced by over 49% compared with the proposed method, the frequency deviations during [40 s, 60 s] are not controlled effectively with the unbounded adaptive ETC scheme and exceed the allowable range (0.2 Hz) during [80 s, 100 s].

Table 3 Performance indices of different control methods (random power fluctuation scenario)

Control schemes	$S^2_{\Delta f}$ (Hz^2)	Triggered times	IAE (Hz·s)
Proposed method	0.0053	156	0.05662
PTC without considering saturations [27]	0.0045	1000	0.05350
PTC considering saturations [26]	0.0045	1000	0.05393
FTETC without considering saturations [23]	0.0058	213	0.06031
FTETC considering saturations	0.0062	163	0.06307
UAETC without considering saturations [25]	0.0061	93	0.06028
UAETC considering saturations	0.0063	75	0.06400

This is because the triggered values in the unbounded adaptive ETC methods increase rapidly when the frequency deviations start to be damped. In this case, the triggered difficulty will be improved which causes the monitoring sensitivity of MG control center for the frequency deviations to be degenerated. Therefore, the proposed bounded adaptive ETC scheme has a better recovery ability for the frequency deviation than existing ETC methods.

4.2 Influence of ESSs and delays on control performance

In this subsection, the influence of ESSs and delays on control performance are further discussed from physical and cyber perspectives.

4.2.1 Influence of ESSs on frequency stability

To verify the contributions of VSG-controlled ESSs to the frequency stability of the islanded MG system, the following three scenarios are simulated and discussed.

Scenario 1 Only the diesel generators are used as the frequency regulation device.

Scenario 2 The diesel generators and ESSs with constant-power control scheme [16] are used as the frequency regulation devices.

Scenario 3 The diesel generators and VSG-controlled ESSs are used as the frequency regulation devices (the framework adopted in this paper).

Assuming that the LFC systems in the above three scenarios adopt the proposed bounded adaptive ETC scheme, all the above three scenarios are tested under the random external power fluctuations as shown in Fig. 6. Figure 11 shows the frequency responses in different scenarios. The triggered intervals are presented in Fig. 12, and Table 4 demonstrates the corresponding control performance indices.

According to Fig. 11 and Table 4, there exists no significant difference of triggered times in the three scenarios. Compared with Scenario 1, the frequency deviation variance and IAE index with auxiliary VSG-controlled ESSs participated in LFC are reduced by 27.40% and 15.87%, respectively. Compared with Scenario 2, the above two performance indices with the proposed LFC framework are reduced by 13.11% and 6.67%, respectively. In addition, from Fig. 10, it can be seen that the frequency deviations in Scenario 1 exceed the allowable range during [20 s, 40 s] and [80 s, 100 s]. Similarly, in Scenario 2, the frequency over-limitation occurs during [80 s, 100 s]. For the proposed LFC framework, the frequency deviations are always within the permitted range (i.e., [−0.2 Hz, 0.2 Hz]). This is because the VSG-controlled ESSs provide not only adjustable regulation capability but also inertia support for the LFC system. Therefore, the simulation results show that the proposed method has a stronger frequency stability in the presence of external power uncertainties.

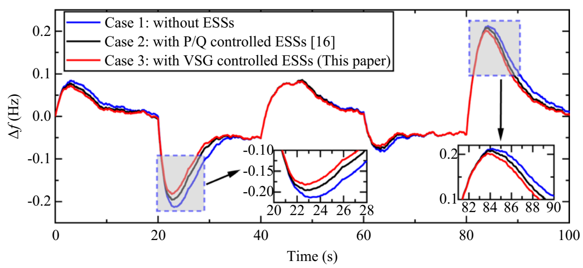

Fig. 11 Frequency deviations in different scenarios

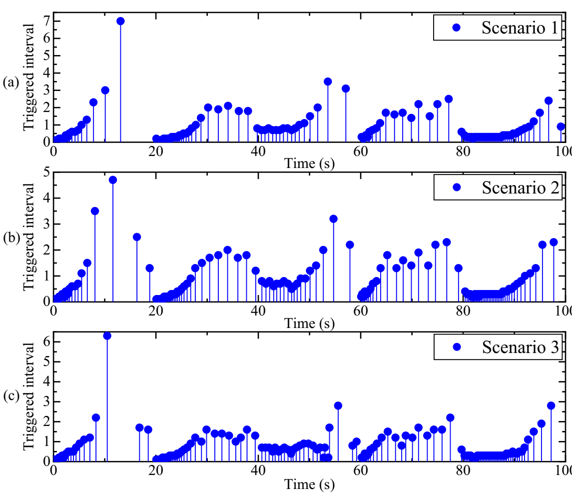

Fig. 12 Triggered intervals in different scenarios

Table 4 Performance indices in different scenarios

Scenarios	(Hz^2)	Triggered times	IAE (Hz·s)
1	0.0073	141	0.06730
2	0.0061	144	0.06066
3	0.0053	156	0.05662

4.2.2 Influence of delays on frequency stability

The robustness of the proposed method with different transmission delays is simulated and discussed. Assuming that the external power disturbance $w(t)$ has a -0.2 p.u. step change a $t=0$ s, Figs. 13 and 14 illustrate the frequency deviations and triggered intervals with different bounded transmission delays, respectively.

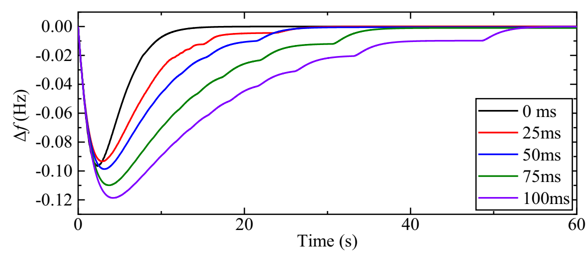

Fig. 13 Frequency deviations with different transmission delays

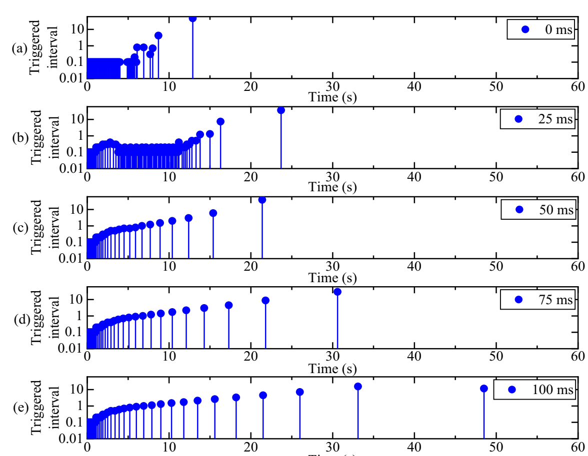

Fig. 14 Triggered intervals with different transmission delays

It can be seen that with the increase of transmission delays, the frequency deviation restoration time is gradually prolonged. In addition, the IAE of frequency deviations rises by 22.65% when the maximum delay increases from 0 to 100 ms. This means that the transmission delays can lead to decreased frequency stability. However, since the optimization algorithm proposed in this paper takes minimizing the frequency deviation amplitude as one of the optimization objectives, the maximum frequency deviation under each delay scenario does not exceed the allowable range. The simulation results show that the proposed bounded adaptive event-triggered LFC scheme and the corresponding optimization algorithm can guarantee satisfactory control performance in heavy network load scenarios.

5 Conclusions

For the LFC issue in an islanded MG, a bounded adaptive event-triggered control scheme considering the spinning reserve constraints has been proposed in this paper. By designing a bounded adjustment mechanism for the triggered threshold, sensitive monitoring ability for the LFC systems and low dependence on network resources can be guaranteed simultaneously. The analytical relations among spinning reserve constraints, uncertain communication delays and ETC parameters have been deduced via constructing the Lyapunov function. Furthermore, an ETC parameter optimization algorithm has been developed to provide optimal balance and compromise between network bandwidth utilization and control performance. Simulation results demonstrate that frequency stability using the proposed method can be enhanced. In the future, the adaptive event-triggered LFC strategy considering spinning reserves, cyber-attacks and more control performance constraints will be further investigated.

Abbreviations

MG	Microgrid
ETC	Event-triggered control
LFC	Load frequency control
VSG	Virtual synchronous generator
ESS	Energy storage system
BLMI	Bilinear matrix inequality
PTC	Periodic triggered control
FTETC	Fixed-threshold ETC
UAETC	Unbounded adaptive ETC

Acknowledgements
Not applicable.

Author contributions
YZ and CP contributed to the conception and design of the study. All authors listed have made a substantial, direct and intellectual contribution to this paper for publication.

Funding
This work was supported in part by the National Natural Science Foundation of China under Grants 62173218, 61833011, 62103254, and the International Corporation Project of Shanghai Science and Technology Commission under Grant 21190780300.

Availability of data and materials
The raw data supporting the conclusions of this article will be made available by the authors, without undue reservation.

Declarations

Competing interests
The authors declare that they have no known competing financial interests or personal relationships that could have appeared to influence the work reported in this paper.

Received: 22 November 2022 Accepted: 19 June 2023
Published online: 06 July 2023

References

1. Mi, Y., Chen, B., Cai, P., He, X., Liu, R., & Yang, X. (2022). Frequency control of a wind-diesel system based on hybrid energy storage. *Protection and Control of Modern Power Systems, 7*(31), 1–13.
2. Zhong, C., Lv, Y., & Li, H. (2021). An equivalent rotor speed compensation control of PMSG-based wind turbines for frequency support in islanded microgrids. *Frontiers in Energy Research, 9*(717327), 1–13.
3. Kumar, S., Josep, G., & Prakash, R. (2022). Robust frequency control in interconnected microgrids: An H_2/H_∞ control approach. *IEEE Systems Journal, 16*(2), 2044–2055.
4. Ali, R., Yazdan, B., Farahnaz, A., & Hassan, B. (2021). Robust load-frequency control in islanded microgrids: Virtual synchronous generator concept and quantitative feedback theory. *IEEE Transactions on Power Systems, 36*(6), 5408–5416.
5. Mohammad, K., Jignesh, S., Sarika, K., & Arman, S. (2021). Stochastic secondary frequency control of islanded microgrid under uncertainties. *IEEE Systems Journal, 15*(1), 1056–1065.
6. Badal, F., Das, P., Sarker, S., & Das, S. (2022). A survey on control issues in renewable energy integration and microgrid. *Protection and Control of Modern Power Systems, 4*(8), 1–27.
7. Firuzi, M., Roosta, A., & Gitizadeh, M. (2021). Stability analysis and decentralized control of inverter-based ac microgrid. *Protection and Control of Modern Power Systems, 4*(6), 1–24.
8. Roozbehani, S., Hagh, M., & Zadeh, S. (2019). Frequency control of islanded wind-powered microgrid based on coordinated robust dynamic droop power sharing. *IET Generation, Transmission and Distribution, 13*(21), 4968–4977.
9. Navid, V., Hassan, K., Tomislav, D., Jalil, B., & Hassan, A. (2019). Time-delayed stabilizing secondary load frequency control of shipboard microgrids. *IEEE Systems Journal, 13*(3), 3233–3241.
10. Anuoluwapo, G., & Kumar, S. (2021). Load frequency control of a two-area power system with a stand-alone microgrid based on adaptive model predictive control. *IEEE Journal of Emerging and Selected Topics in Power Electronics, 9*(6), 7253–7263.
11. Zhang, C., Dou, X., Zhang, Z., Lou, G., Yang, F., & Li, G. (2021). Inertia-enhanced distributed voltage and frequency control of low-inertia microgrids. *IEEE Transactions on Power Systems, 36*(5), 4270–4280.
12. Tuffner, F., Schneider, K., Hansen, J., & Elizondo, M. (2019). Modeling load dynamics to support resiliency-based operations in low-inertia microgrids. *IEEE Transactions on Smart Grid, 10*(3), 2726–2737.
13. Pilehvar, M., & Mirafzal, B. (2020). Frequency and voltage supports by battery-fed smart inverters in mixed-inertia microgrids. *Electronics, 9*(11), 1–14.
14. Arani, Z., Taher, S., Ghasemi, A., & Shahidehpour, M. (2019). Application of multi-resonator notch frequency control for tracking the frequency in low inertia microgrids under distorted grid conditions. *IEEE Transactions on Smart Grid, 10*(1), 337–349.
15. Jia, H., Li, X., Mu, Y., Xu, C., Jiang, Y., Yu, X., Wu, J., & Dong, C. (2018). Coordinated control for ev aggregators and power plants in frequency regulation considering time varying delays. *Applied Energy, 210*, 1363–1376.

16. Samy, A., Senthil, N., & Gonzalez-Longatt, F. (2019). Robust PI controller design for frequency stabilisation in a hybrid microgrid system considering parameter uncertainties and communication time delay. *IET Generation, Transmission and Distribution, 13*(14), 3048–3056.
17. Fathin, S., Thongchart, K., Masayuki, W., & Yasunori, M. (2019). Optimization of virtual inertia considering system frequency protection scheme. *Electric Power Systems Research, 170*, 294–302.
18. Naderi, M., Shafiee, Q., Bevrani, H., & Blaabjerg, F. (2021). Low-frequency small-signal modeling of interconnected ac microgrids. *IEEE Transactions on Power Systems, 36*(4), 2786–2797.
19. Zhang, Y., Peng, C., Xie, S., & Du, X. (2022). Deterministic network calculus-based H_∞ load frequency control of multiarea power systems under malicious dos attacks. *IEEE Transactions on Smart Grid, 13*(2), 1542–1554.
20. Markovic, U., Stanojev, O., Aristidou, P., Vrettos, E., Callaway, D., & Hug, G. (2021). Understanding small-signal stability of low-inertia systems. *IEEE Transactions on Power Systems, 36*(5), 3997–4017.
21. Dong, L., Tang, Y., He, H., & Sun, C. (2017). An event-triggered approach for load frequency control with supplementary ADP. *IEEE Transactions on Power Systems, 32*(1), 581–589.
22. Lou, G., Hong, Y., Gu, W., & Xie, J. (2022). Distributed event-triggered multi-timer synchronization scheme for secondary control in islanded microgrids. *International Journal of Electrical Power and Energy Systems, 135*, 1–12.
23. Shangguan, X., He, Y., Zhang, C., Jin, L., Yao, W., Jiang, L., & Wu, M. (2022). Control performance standards-oriented event-triggered load frequency control for power systems under limited communication bandwidth. *IEEE Transactions on Control Systems Technology, 30*(2), 860–868.
24. Peng, C., & Yang, T. (2013). Event-triggered communication and H_∞ control co-design for networked control systems. *Automatica, 49*(5), 1326–1332.
25. Lu, K., Zeng, G., Luo, X., Weng, J., Zhang, Y., & Li, M. (2020). An adaptive resilient load frequency controller for smart grids with dos attacks. *IEEE Transactions on Vehicular Technology, 69*(5), 4689–4699.
26. Yang, T., Zhang, Y., Li, W., & Zomaya, A. (2020). Decentralized networked load frequency control in interconnected power systems based on stochastic jump system theory. *IEEE Transactions on Smart Grid, 11*(5), 4427–4439.
27. Anirban, S., & Dushmanta, K. (2021). Mitigating inter-area oscillation of an interconnected power system considering time-varying delay and actuator saturation. *Sustainable Energy, Grids and Networks, 27*, 1–10.
28. Fathi, A., Shafiee, Q., & Bevrani, H. (2018). Robust frequency control of microgrids using an extended virtual synchronous generator. *IEEE Transactions on Power Systems, 33*(6), 6289–6297.
29. Khalghani, M., Solanki, J., Solanki, S., & Sargolzaei, A. (2021). Stochastic secondary frequency control of islanded microgrid under uncertainties. *IEEE Systems Journal, 15*(1), 1056–1065.
30. Oshnoei, A., Kheradmandi, M., & Muyeen, S. (2020). Robust control scheme for distributed battery energy storage systems in load frequency control. *IEEE Transactions on Power Systems, 35*(6), 4781–4791.
31. Wang, Y., Xu, Y., Tang, Y., Liao, K., Syed, M., Guillo-Sansano, E., & Burt, G. (2019). Aggregated energy storage for power system frequency control: A finite-time consensus approach. *IEEE Transactions on Smart Grid, 10*(4), 3675–3686.
32. Gu, K., Kharitonov, V., & Chen, J. (2003). *Stability of time-delay systems*. Birkhauser.
33. Park, P., Ko, J., & Jeong, C. (2011). Reciprocally convex approach to stability of systems with time-varying delays. *Automatica, 47*(1), 235–238.
34. Ge, X., Han, Q., & Wang, Z. (2019). A threshold-parameter-dependent approach to designing distributed event-triggered H_∞ consensus filters over sensor networks. *IEEE Transactions on Cybernetics, 49*(4), 1148–1159.
35. Singiresu. S. (2009). Engineering optimization theory and practice.

Yajian Zhang (1991-), male, Ph.D., Major in the secure networked control systems, power cyber-physical systems and power grid security control.

Chen Peng (1972-), male, Ph.D. and Professor, Major in the networked control systems, distributed control systems, smart grid, and intelligent control systems.